Ancilla-entangling Floquet kicks for accelerating quantum algorithms

C.-C. Joseph Wang, Phillip C. Lotshaw, Titus Morris, Vicente Leyton-Ortega, Daniel Claudino, and Travis S. Humble

Phys. Rev. A **111**, L010401 — Published 3 January 2025

DOI: 10.1103/PhysRevA.111.L010401

Ancillary entangling Floquet kicks for accelerating quantum algorithms

C.-C. Joseph Wang, Phillip C. Lotshaw, Titus Morris, Vicente Leyton-Ortega, Daniel Claudino, and Travis S. Humble
Quantum Computational Science Group, Quantum Information Science Section,
*Oak Ridge National Laboratory, 1 Bethel Valley Road, Oak Ridge, 37831, TN, USA**
(Dated: November 21, 2024)

Quantum simulation with adiabatic annealing can provide insight into difficult problems that are impossible to study with classical computers. However, it deteriorates when the systems scale up due to the shrinkage of the excitation gap and thus places an annealing rate bottleneck for high success probability. Here, we accelerate quantum simulation using digital multi-qubit gates that entangle primary system qubits with ancillary qubits. The practical benefits originate from tuning the ancillary gauge degrees of freedom to enhance the quantum algorithm's original functionality in the system registry. For simple but nontrivial short-ranged, infinite long-ranged transverse-field Ising models, and the hydrogen molecule model after qubit encoding, we show improvement in the time to solution by one hundred percent but with higher accuracy through exact state-vector numerical simulation in a digital-analog setting. The findings are further supported by time-averaged Hamiltonian theory.

PACS numbers: 03.67.Lx; 03.67.a; 03.65.Ud; 06.20.Dk; 07.05.Kf
Keywords: Quantum simulation, quantum algorithm, quantum annealing, and quantum error suppression

Classical simulation of quantum many-body systems is incredibly difficult because of the many degrees of freedom (DOF) involved [1]. To solve this problem, quantum analog simulation with adiabatic annealing has been used, which requires less strict controls for implementation [2–4]. However, due to the critical slowdown caused by the decrease in the minimal excitation gap as the quantum system becomes larger [5], the initial success of adiabatic quantum annealing protocols in small quantum systems [6, 7] is not expected to continue at a larger scale due to the upper bound of the coherence time set by quantum hardware and the condition to stay adiabatic. Digital quantum simulations [8] have become the mainstream to sidestep the limitation.

More recently, digital simulations through hybrid variational quantum algorithms (HVQAs) with classical optimization show great promise for realizing applications [9–15] due to their universality (in computation) and the potential to demonstrate quantum advantage in practical tasks. However, with overparametrized circuits, HVQAs also suffer from many problems inherited from classical optimization [16–20]. To leverage practical values from current noisy quantum computing hardware [21] toward quantum utility, diverse universal quantum computing paradigms—involving the programmable analog model, gate models, digital-analog models, and measurement-based feedforward model—are actively pursued [22–29]. The race to design practical quantum algorithms (heuristic or deterministic) compatible with diverse paradigms and platforms for realizing practical quantum applications at scale remains critical. We show that quantum simulations can be accelerated with optimal quantum kicks, requiring only single parameter optimization offline (insensitive to system size) and utilizing limited resources of ancillary qubits while preserving the quantum information in the system qubits where the core quantum application operates.

We adopt a quantum annealer as the quantum optimizer with encoded applications in the system-only Hamiltonian. The quantum annealer can overcome the local minima traps by exploring the system energy landscape with mixer system Hamiltonian through quantum tunneling [30]. It is theoretically equivalent to the quantum approximate optimization algorithm after dense Trotterization in a finite simulation time. However, the annealer faces a significant drawback due to the finite excitation gap of the encoded Hamiltonian not being large enough for the annealing time scale. Thus the quantum dynamics cannot follow the desired adiabatic state evolution for the system Hamiltonian at a faster annealing. Although counter-diabatic Hamiltonian approaches have been proposed to counter the diabatic effects, the complexity of the nested counter-diabatic terms makes these approaches hard to implement in practice [31–34]. To address this issue, we propose a new quantum protocol to accelerate quantum simulation by controlling nonadiabatic quantum state evolution with additional ancillary qubits. We achieve this by designing entangling gates with periodic (Floquet) kicks that deviate state evolution from the adiabatic path early in the simulation but allow the passage back to the target quantum path shortly after.

Firstly, we enlarge the primary system Hilbert space S with the secondary ancillary Hilbert space A. The quantum computation is enabled by the always-on *system* unitary $U^S(t)$ that encodes the interested problem in analog quantum simulation and the digital quantum kick unitaries $U^{SA}(\hat{\Theta}^A, \hat{S}) = \exp(-i\hat{\Theta}^A \otimes \hat{S})$ that accelerate the quantum simulation. The operator $\hat{\Theta}^A$ and the collective system operator $\hat{S} = \sum_{l=1}^{N_S} \sigma_l^S$ (with N_S system qubits) act on the A space and S space respectively. The choice of $\hat{\Theta}^A$ is not unique but can be limited to sim-

ple forms with minimal compilation for target quantum simulation. We initialize the ancillary state as a product state right at the outset for the quantum simulation before the entanglement with the system qubits enabled by $U^{SA}(t)$. In qubit language, the corresponding operator $\hat{\Theta}^A$ is given by

$$\hat{\Theta}^A = \sum_{l=1}^{N_A} \theta_l \sigma_l^A \tag{1}$$

where the Pauli operators σ_l^A for qubit l are selected from the gate set $\{X_l^A, Y_l^A, Z_l^A\}$ and the summation is over N_A ancillary qubits. For ground-state properties, the target function to minimize is the reduced system energy in S : $Tr_S(\hat{\rho}^S(t)H^S(t))$ after the repetitive action of the identical kick unitary operator $U^{SA}(\hat{\Theta}^A, \hat{S})$ acting on the state $\hat{\rho}^{SA}(t-\epsilon)|_{\epsilon\to 0^+} := |\psi^{SA}(t-\epsilon)\rangle\langle\psi^{SA}(t-\epsilon)|$ governed by the always-on system Hamiltonian $H^S(t)$ right before the quantum kick. For the simplicity of notation, we chose $\hbar = 1$ as our unit system so that we can drop $\hbar$ and the system Hamiltonian and the rest in our further discussion have the dimension [radians/time]. The overall quantum state evolves as $\hat{\rho}^{SA}(t) = U^{\dagger SA}(t)\rho^{SA}(t-\epsilon)U^{SA}(t)$ with the reduced system state after tracing out ancillary subsystem as $\hat{\rho}^S(t) = Tr_A\hat{\rho}^{SA}(t)$. To have a low-cost compilation, we set our smart gate parameters θ_l to be a single uniform parameter θ for the simplest gate design with one spin orientation selected from the ancillary Pauli operator set $\{X_l^A, Y_l^A, Z_l^A\}$.

Secondly, the choices of efficient multi-qubit quantum kicks—up to a local unitary rotation in A (gauge DOF)—depend on the encoded quantum simulation applications. The quantum kick gate sets shall be selected as those with good sensitivity to change the reduced system energy landscape $Tr_S\left(\hat{\rho}^S H^S(t)\right)$ and meet the non-commuting relation $[\sigma_i^S, H^S(t=0)] \neq 0$ and the commutation relation $[\sigma_i^S, H^S(t=T)] = 0$ at the end of simulation time T. Guided by numerical studies from our in-house state-vector simulator and theoretical studies with time-averaged Hamiltonian theory [38–40]—based on leading-order Magnus expansion in the strong rotating reference frame from the trivial transverse-field (mixer) Hamiltonian. In digital-analog settings, we identify that discrete entangling quantum kicks are instrumental in accelerating applications when the quantum kick strength is optimally upper-bounded without causing nonadiabatic excitations.

Optimal kick angle estimation.— We theoretically estimate the optimal kick angle θ_{opt} based on the non-perturbative time-averaged Hamiltonian approach. The theory estimation reconciles with the numerical results from the state-vector simulation. The optimal kick angle to stay close to the system ground state energy for the quantum kicks, is given by the following expression (See details in [47]) for the transverse field Ising models (TFIMs) and the H_2 molecule model for describing quantum dynamics before dynamical quantum phase transition (QPT) with a theory cutoff $T \approx \tau$:

$$\theta_{opt} \approx \frac{1}{N_A N_K}\sqrt{1 - E_S^T/E_S^{Mixer}(\tau)}, \tag{2}$$

in which E_S^T is the true system ground state energy and $E_S^{Mixer}(T=\tau)$ is the system mixer energy. The formula is based on the numerical observation for circumstances with over-kicking angles that cause reduced system energy overshoot above true system ground state energy before QPT, it never ends up closer to the true ground state energy. The expression is valid and universal as long as the mixer Hamiltonian and the kick Hamiltonian are the *only* dominant [47] Hamiltonian for the proposed quantum kick algorithm since the specifics of the system Hamiltonian will not contribute much to quantum state evolution before QPT. As follows, we will validate the ideas through transverse-field quantum Ising models essential for benchmarking quantum simulation for quantum materials, hybrid quantum-classical algorithms and quantum combinatorial optimization [35](its generalization is universal for simulating exotic quantum phases [36]) and the hydrogen molecule model, the fundamental building block for quantum chemistry problems.

Nearest-neighbor transverse field Ising model (NN-TFIM) in an open chain.— It is well understood that a QPT occurs for the NN-TFIM [37] with a finite excitation gap Δ_{min} that sets the bound to the simulation time to solution. With the kick protocol, we can speed up the passage through the QPT even at a faster annealing rate than Δ_{min}^{-1}. The schedule for the system Hamiltonian $H^S(t)$ with the end simulation time T is given by:

$$H^S(t) = \underbrace{\sum_i \theta_M(t) Z_i^S}_{H_M^S(t)} + \underbrace{\sum_{\langle i<j\rangle} -\theta_{XX}^0 X_i^S X_j^S}_{H_P^S}, \tag{3}$$

in which $\theta_{XX}^0 > 0$ and H_M^S is the one-local mixer Hamiltonian in S space with the positive amplitude $\theta_M(t) = \theta_Z^0(:= \theta_M(0))e^{-t/\tau}$ following the spatially uniform annealing with the time constant τ. The always-on negative uniform Ising interaction $-\theta_{XX}^0$ between system qubits favors the GHZ ground state $|\mathrm{GHZ}\rangle = 1/\sqrt{2}(|0_x\rangle^{\otimes N_S} + |1_x\rangle^{\otimes N_S})$ for the system problem Hamiltonian H_P^S. With the chosen parameters $\theta_Z^0/\theta_{XX}^0 = 5.0$, the model is initialized at the ground state in proximity to the product state $|1\rangle^{\otimes N_S}$ for the system qubits and $|0\rangle^{\otimes N_A}$ for the ancillary qubits.

The summation of the probability measured at the computational basis $|0\rangle^{\otimes N_S}$ and $|1\rangle^{\otimes N_S}$ is provided as the proxy for the ferromagnetic order (polarized state) in the basis and abbreviated as PFM. We expect that, with faster annealing ($\Delta_{min}\tau > 1$), diabatic transitions are not negligible and limit the time scale τ to reach the true target ground state. This is the critical slowdown effect.

However, this is not the problem with a large transverse field at the initial stage of the quantum simulation with a large excitation gap proportional to θ_Z^0.

To speed up the simulation, we can apply an efficient quantum kick that does not commute with the trivial mixer Hamiltonian $H_M^S(t)$ at the kick time with a properly chosen ancillary and system Pauli operators σ_l^A and σ_l^S at this early stage in which the diabatic effects are suppressed mostly. In Fig. 1, we show the efficient digital kick Hamiltonian $H^{SA}(t) = \theta(t)\sum_{ij} X_i^S \otimes Z_j^A$ at time t with Dirac kicks $\theta(t) := \theta\sum_{K=0}^{N_K-1}\delta(t-K\Delta t_K)$ in which N_K is the accumulated number of kicks before time t and θ is the kick angle in radians. The impulsive kicks intercept periodically with the always-on system Hamiltonian $(H_P^S + H_M^S)$ with a given kick angle θ immediately after the state preparation. In the numerical simulation, the optimal kick angle θ_{opt} is found empirically by grid searched results, and is found later in excellent agreement [47] with the theory estimation from the time-averaged Hamiltonian [38, 39]. We differentiate the efficiency of kicks by the sensitivity response of the system to each type of kicks [48]. The system Pauli operator X_i^S is chosen because it does not commute with the instant mixer Hamiltonian $H_M^S(t)$ in S but commutes with the target Hamiltonian H_P^S in S. For the most efficient ancillary operator in A subspace, we need to choose $\sum_{ij} X_i^S \otimes X_j^A$ or $\sum_{ij} X_i^S \otimes Z_j^A$ with the most pronounced landscape instead of the flattened one $\sum_{ij} X_i^S \otimes Y_j^A$, which requires a stronger kick angle to reach the same speedup.

In practice, it is hard to determine precisely what the optimal kick angle value $\theta := \theta_{opt}$ is to avoid excess excitations, and to have a reliable simulation at the end but to run experiments at different system sizes. In Fig. 1, our numerical demonstration shows the periodic kick Hamiltonian $\theta(t)\sum_{ij} X_i^S \otimes Z_j^A$ with $N_K = 43$, $\theta_{opt} = 0.004$ (in radians) spanning the duration $t \lesssim \tau$. The reduced system energy is calculated after tracing out ancillary DOF with the kicks. The true ground state energy is calculated with imaginary time evolution in *S-only* subspace.

In subplots 1(a) and 1(b) for the slower annealing $\Delta_{min}\tau \approx \theta_{XX}^0\tau = 0.5$, the system dynamics reaches the same reduced system energy faster. As a byproduct, the speedup lifts the reduced system energy from the true ground-state energy floor at the end of the simulation. For the Floquet quantum kicks with larger θ (not shown), excited quantum states can lead to very wrong answers at the end of the quantum simulation. For a much weaker kick angle $\theta \ll 0.004$ (not shown), we cannot achieve any benefits from the kicks as opposed to the case without the kicks.

In subplots 1(c) and 1(d) with the faster annealing $\theta_{XX}^0\tau = 0.25$ and high-frequency kicks, the excess excitations are suppressed and lead to the right drift to the true ground state system energy [49]. The time to the steady state for the reduced system energy is much shorter (one hundred percent reduction) signaling the acceleration to the target ground state system energy. The drawback from excess excitations is completely negated with the high-frequency ($\theta_Z^0\Delta t_K \ll 1$ and $\theta_{XX}^0\Delta t_K \ll 1$) quantum kicks.

In subplots 1(e)-1(h) illustrated is the reduced system dynamics from the system Hamiltonian $H^S(t)$ and the continuous constant kick Hamiltonian $\theta(t)\sum_{ij} X_i^S Z_j^A$ spanning the whole simulation time T, the kicks always drive the system energy closer to the true system energy even at faster annealing. However, the speedup is still effective (with less error and faster convergence to final results than the case without kicks) at a slower or faster annealingtime τ (as shown in subplots 1(e-f) versus 1(g-h)). It is encouraging for the NN-TFIMs that the optimal kick angle is not sensitive to the system size for the quantum kick protocol.

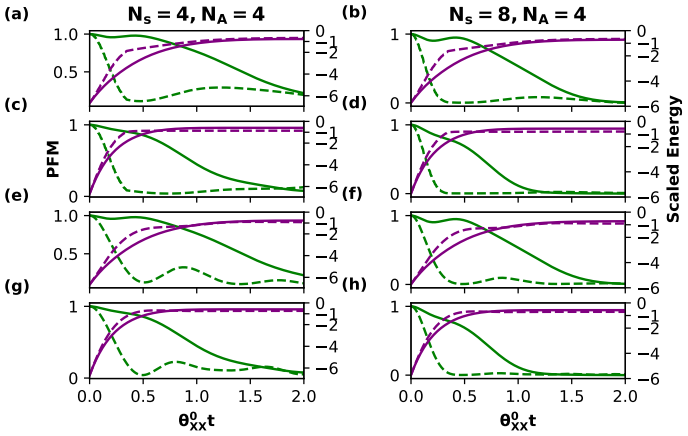

FIG. 1: NN-TFIM in an open chain with $\theta_{XX}^0 = 1.0$, $\theta_M(0) = \theta_Z^0 = 5\theta_{XX}^0$: time dependency of the projected probability PFM in the ground state for the mixer Hamiltonian $|1\rangle^{\otimes N_S}$ (in green color with values given by the left side ticks) and the scaled system energy (in purple with values given by the right side ticks) computed by the ratio between the reduced system energy and the absolute value of the true system ground-state energy. The purple solid lines present the cases without the kicks $\theta = 0$. The green lines (dashed ones with kicks and solid ones without kicks) are the proxy for the disappearance of the ferromagnetic order along the Pauli-X orientation. All cases with solid (dashed) lines represent the cases without (with) any types of kicks. Floquet kicks with the same kick angle $\theta = 0.004$ (in radians) and the kick time interval Δt_K between kicks is related to the Ising interaction $\theta_{XX}^0\Delta t_K = 0.0008$. (a) $\theta_Z^0\tau = 0.8^{-1}$, (b) $\theta_Z^0\tau = 0.8^{-1}$, (c) $\theta_Z^0\tau = 1.6^{-1}$, (d) $\theta_Z^0\tau = 1.6^{-1}$. Continuous weak kicks with the constant kick angle $\theta \to 0, N_K \to \infty$: (e) $\theta_Z^0\tau = 0.8^{-1}$, (f) $\theta_Z^0\tau = 0.8^{-1}$, (g) $\theta_Z^0\tau = 1.6^{-1}$, (h) $\theta_Z^0\tau = 1.6^{-1}$.

Infinite long-ranged transverse field Ising model (ILR-TFIM) in a closed chain.— To study the effect with a similar gap size near QPT as the NN-TFIM, we rescale

the Ising interaction θ^0_{XX} to the lower value of $\theta^0_{XX} \to \theta^0_{XX}/(0.5N_S)$ while keeping the same θ^0_Z, in which the scaling factor $0.5N_S$ is given by the ratio of the connectivity between ILR-TFIM:$N_S(N_S-1)/2$ and NN-TFM: $N_S - 1$. The robustness of the quantum kick protocol prevails with the ILR-TFIM system Hamiltonian $H_P^S = -\sum_{i<j} \theta^0_{XX} X_i^S X_j^S$ [52].

Hydrogen molecule model.— Due to the fermionic parity symmetry inherent to the low-energy valence electrons in a hydrogen molecule (H_2), the H_2 quantum state is encoded by two spins after the Bravyi-Kitaev transformation [41, 42] and tapering [43, 44]. The relevant low-energy subspace is spanned by $|01\rangle$ and $|10\rangle$ basis states. The system Hamiltonian is given by the linear combination of the Pauli terms $I_0^S I_1^S$, $Z_0^S Z_1^S$, $I_0^S Z_1^S$, $Z_0^S I_1^S$, and $X_0^S X_1^S + Y_0^S Y_1^S$ with given coupling interaction for different bond lengths shown in H_2 data [51]. H_2 system Hamiltonian commutes with $\sum_i Z_i^S$ due to the parity conservation. If we initiate the quantum state at $|01\rangle$ or $|10\rangle$, the H_2 Hamiltonian will not change parity, the eigenvalue of $\sum_i Z_i^S$. By our proposed protocol, we need a mixer Hamiltonian not commuting with H_2 system Hamiltonian that can facilitate the superposition between states with different parities initially and does not lead us astray to the excited states. Therefore, we need a one-local system mixer Hamiltonian that is not $\theta_M(t)\sum_i Z_i^S$ but the mixer $\theta_M(t)\sum_i X_i^S = \theta^0_X e^{-t/\tau}\sum_i X_i^S$ and carry out the quantum simulation with annealing. For the choice of an efficient quantum kick, we select the instantaneous kick Hamiltonian commuting with the relevant H_2 system Hamiltonian $X_0^S X_1^S + Y_0^S Y_1^S$, we can still speed up the quantum simulation as TFIMs and find the exact ground state energy for H_2 with the protocol. As one observes [52], this is not the most efficient kick but still reaches the simulation goal with a larger optimal kick angle θ. The efficient quantum kick unitary $U^{SA}(\hat{\Theta}^A, \hat{S})$ for the H_2 molecule model is chosen with the ancillary operator $\hat{\Theta}^A = \theta\sum_l Z_l^A$ and system operator $\hat{S} = \sum_i \frac{1}{\sqrt{2}}(X_i^S + Y_i^S)$ respectively.

Following the schedule Eq. (3) with the problem Hamiltonian H_P^S replaced by the H_2 Hamiltonian, we illustrate our numerical speedup results in Fig. 2 and Fig. 3 for distinct bond length and interaction in atomic units [51]. The full quantum state is initialized at the product state $|1_x\rangle^{\otimes 2} \bigotimes |1_x\rangle^{\otimes N_A}$, in which $|1_x\rangle^{\otimes 2}$ is the ground state for the mixer Hamiltonian $\theta^0_X \sum_i X_i^S$. It is noted that the sampled kick angles θ shown are not near optimal for any annealing rate.

In Fig. 2 ($N_A = 2$, bond length = 2.0 $a.u$) and Fig. 3 ($N_A = 6$, bond length = 2.0 $a.u$), all purple energy curves collapse to the right binding energies at the long time limit. However, not all kick angles (fast or slow annealing rates) have the advantage over the case without the kick ($\theta = 0$), especially the case $\theta^0_X\tau = 0.18^{-1}$ with fast annealing in Fig. 3. For the cases with hydrogen bond

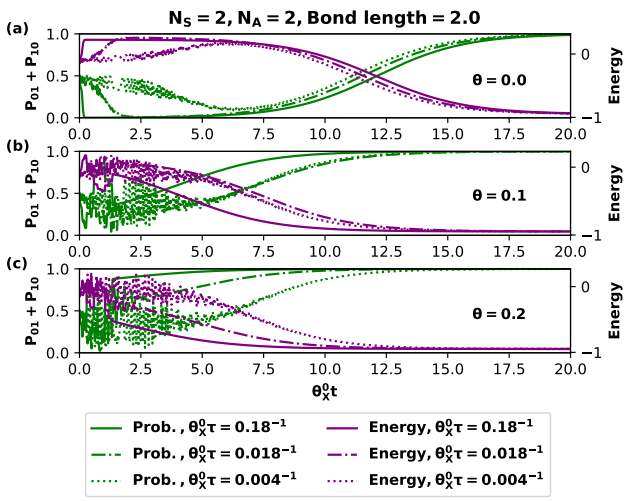

FIG. 2: Time dependency of probability in odd parity subspace $|01\rangle$ and $|10\rangle$ (in green) and H_2 system binding energy (in purple) with $N_S = 2$, $N_A = 2$, bond length = 2.0$a.u.$, and $\theta^0_X = 1.5$. The annealing rates $\theta^0_X\tau$ are shown in the attached legend. Different line types present cases with different annealing rates. The kick angle $\theta = 0$ labels the cases without the kicks in the top subplot (a). The tick values at the left vertical axis mark the values for the probability measurement cases (green), and those marked at the right vertical axis are for the energy measurement (purple).

length 0.7 $a.u.$ [53], we also observe the convergence to the true binding energy for any annealing rate. Still, with the clear advantages of the kicks, we show the kick angle dependence is not monotonic concerning the annealing rates due to the over-rotation of the same kick angles for excitations with more ancillary qubits. We also observe the much shortened time $\theta^0_X t$ to the true system binding energy.

In summary, we have developed a quantum speedup protocol using a digital-analog computing framework for quantum simulations bypassing the gap bottleneck of quantum simulation through adiabatic annealing. The protocol can be broadly applied for any quantum applications after Hamiltonian encoding including quantum sensing, quantum optimization [45], quantum machine learning [46], and quantum state preparation [55].

Our method demonstrates one hundred percent speedup (with respect to cases without kicks) in considered NN-TFIM, ILR-TFIM, and H_2 models by applying quantum annealing algorithms with specific quantum kicks, particularly useful for simulations in noisy quantum hardware with short coherence time. Our design work also builds upon existing quantum algorithms and could be easily adapted to current or next-generation programmable digital-analog quantum devices in the lab. The quantum speedup primitive is novel from the standpoint of the modular algorithm design principle, without changing the core algorithms in the system space.

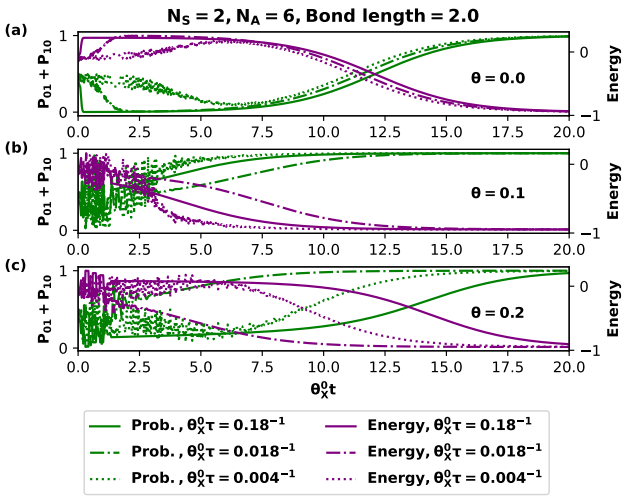

FIG. 3: Time dependency of probability in odd parity subspace $|01\rangle$ and $|10\rangle$ and H_2 system binding energy with $N_S = 2$, $N_A = 6$, bond length = 2.0, and $\theta_X^0 = 1.5$. The annealing rates $\theta_X^0\tau$ are shown in the attached legend. The cases without the kicks are labeled by the kick angle $\theta = 0$ in the top subplot.

For an end-to-end quantum application chained through multiple Hamiltonian-encoded subroutines that function differently in an application such as state preparation or quantum information processing, the full algorithm comprises alternating annealing or ramping for the mixer and interested system Hamiltonians intersperse with quantum kicks for each subroutine layer. In each subroutine layer, we potentially can reuse ancillary qubits, and reset the ancillary and system states at each functional layer by measurement and feedforward protocol over the ancillary registry since the quantum information in the system registry is preserved. The ancillary resource remains constant for the increased complexity of the chained quantum subroutines.

The operation of the auxiliary qubits can be potentially influenced by the control errors manifested in the kick angle, coherent noises and incoherent noises in the hardware. However, the fast and weak coherent noises shall be perturbative for the desired outcome from the time average behaviors of the quantum dynamics. The low frequency coherent noises and control errors can offset the kick angle but can be calibrated empirically in advance with very few ancillary qubits. The nonperturbative quantum kicks boost the convergence to the target solution in addition to the native quantum annealing with strong interaction. This shall render the effects from environmental decoherence minimized. With more intended effort, the primitive can potentially be rendered fault-tolerant by various schemes with further studies.

C.-C. Joseph Wang and Travis Humble acknowledge the support by the DOE Office of Science, Office of ASCR, under FWP No. ERKJ354 to initiate the project. The continuation of the project was supported by the U.S. Department of Energy, Office of Science, National Quantum Information Science Research Centers, Quantum Science Center.

* wangccj@ornl.gov;

[1] A. J. Daley, I. Bloch, C. Kokail, S. Flannigan, N. Pearson, M. Troyer, P. Zoller, Nature, **607**, 667–676 (2022).
[2] S. Yarkoni, E. Raponi, T. Bäck, S. Schmitt, Rep. Prog. Phys., **85**, 104001 (2022).
[3] M. Bernaschi, I. González-Adalid Pemartín, V. Martín-Mayor, G. Parisi, Nature, **631**, 749–754 (2024).
[4] A. D. King, J. Raymond, T. Lanting, R. Harris, A. Zucca, F. Altomare, A. J. Berkley, K. Boothby, S. Ejtemaee, C. Enderud et al., Nature, **617**, 61–66 (2023).
[5] S. Knysh, Nat. Commun., **7**, 12370 (2016).
[6] L. Feng, O. Katz, C. Haack, M. Maghrebi, A. V. Gorshkov, Z. Gong, M. Cetina and C. Monroe, Nature, **623**, 713–717 (2023).
[7] R. Islam, C. Senko, W. C. Campbell, S. Korenblit, J. Smith, A. Lee, E.E. Edwards, C.-C. J Wang, J. K. Freericks, C. Monroe, Science, **340**, 583-584 (2013).
[8] S. Lloyd, Science, **273**, 1073-1078 (1996).
[9] S. Endo, Z. Cai, S. C. Benjamin, and X. Yuan, J. Phys. Soc. Jpn., **90**, 032001 (2021).
[10] M. Cerezo, A. Arrasmith, R. Babbush, S. C. Benjamin, S. Endo, K. Fujii, J. R. McClean, K. Mitarai, X. Yuan, L. Cincio et al., Nat. Phys., **3**, 625 (2021).
[11] X. Xu, S. C. Benjamin and X. Yuan, Phys. Rev. Applied, **15**, 034068 (2021).
[12] H. R. Grimsley, S. E. Economou, E. Barnes, N. J. Mayhall, Nat. Commun.,**10**, 3007 (2019).
[13] P. J. J. O'Malley, R. Babbush, I. D. Kivlichan, J. Romero, J. R. McClean, R. Barends, J. Kelly, P. Roushan, A. Tranter, N. Ding, and B. Campbell et al., Phys. Rev. X, **6**, 031007 (2016).
[14] B. F. Schiffer, J. Tura, and J. I. Cirac, PRX Quantum, **3**, 020347 (2022).
[15] J. Biamonte, Phys. Rev. A, **103**, L030401 (2021).
[16] M. Larocca, S. Thanasilp, S. Wang, K. Sharma, J. Biamonte, P. J. Coles, L. Cincio, J. R. McClean, Z. Holmes, M. Cerezo, arXiv:2405.00781.
[17] J. R. McClean, S. Boixo, V. N. Smelyanskiy, R. Babbush, H. Neven, Nat. Commun., **9**, 4812 (2018).
[18] M. Cerezo, A. Sone, T. Volkoff, L. Cincio and P. J. Coles, Nat. Commun., **12**, 1791 (2021).
[19] H.-Y. Liu, Z.-Y. Chen, T.-P. Sun, C. Xue, Y.-C. Wu, G.-P. Guo, arXiv:2307.04089.
[20] L. Bittel and M. Kliesch, Phys. Rev. Lett., **127**, 120502

(2021).
[21] J. Preskill, Quantum, **2**, 79 (2018).
[22] E. Altman, K. R. Brown, G. Carleo, L. D. Carr, E. Demler, C. Chin, B. DeMarco, S. E. Economou, M. A. Eriksson et al., PRX QUANTUM, **2**, 017003 (2021).
[23] M. Iqbal, N. Tantivasadakarn, R. Verresen, S. L. Campbell, J. M. Dreiling, C. Figgatt, J. P. Gaebler, J. Johansen, M. Mills, S. A. Moses, et al., Nature, **626**, 505 (2024).
[24] R. Harris, Y. Sato, A. J. Berkley, M. Reis, F. Altomare, M. H. Amin, K. Boothby, P. Bunyk, C. Deng, C. Enderud et al., Science, **361**, 162 (2018).
[25] D. Bluvstein, S. J. Evered, A. A. Geim, S. H. Li, H. Zhou, T. Manovitz, S. Ebadi, M. Cain, M. Kalinowski, D. Hangleiter et al., Nature, **626**, 58 (2024).
[26] Y. Kim, A. Eddins, S. Anand, K. X. Wei, E. van den Berg, S. Rosenblatt, H. Nayfeh, Y. Wu, M. Zaletel, K. Temme, and A. Kandala, Nature, **618**, 500 (2023).
[27] L. Feng, O. Katz, C. Haack, M. Maghrebi, A. V. Gorshkov, Z. Gong, M. Cetina, and C. Monroe, Nature, **623**, 713 (2023).
[28] S. Bartolucci, P. Birchall, H. Bombín, H. Cable, C. Dawson, M. Gimeno-Segovia, E. Johnston, K. Kieling, N. Nickerson, M. Pant, F. Pastawski, T. Rudolph, and C. Sparrow, Nat. Commun., **14**, 020328 (2023).
[29] T. Gonzalez-Raya, R. Asensio-Perea, A. Martin, L.C. Céleri, M. Sanz, P. Lougovski, and E. F. Dumitrescu, PRX Quantum, **2**, 020328 (2021).
[30] A. Das, Arnab and B. K. Chakrabarti, Rev. Mod. Phys., **80**, 1061 (2008).
[31] P. W. Claeys, M. Pandey, D. Sels, A. Polkovnikov, Phys. Rev. Lett., **123**, 090602 (2019).
[32] A. Hartmann and W. Lechner, New J. Phys., **21**, 043025 (2019).
[33] J. Wurtz and P. J. Love, Quantum, **6**, 635 (2022).
[34] C. M. Keever and M. Lubasch, PRX Quantum, **5**, 020362 (2024).
[35] G. Pagano, A. Bapat, P. Becker, K. S. Collins, A. De, P. W. Hess, H. B. Kaplan, A. Kyprianidis, W. L. Tan, C. Baldwin, L. T. Brady, A. Deshpande, F. Liu, S. Jordan, A. V. Gorshkov, C. Monroe, PNAS, **117**, 25396-25401 (2020).
[36] R. Verresen, arXiv:2301.11917.
[37] S. Sachdev, Quantum Phase Transitions, Cambridge University Press, Second edition (2011).
[38] A. Brinkmann, Concepts Magnetic Resonance. **45A**, e21414 (2016).
[39] S. Blanes, F. Casas, J.A. Oteo, and J. Ros, Physics Reports, **470**, 151 (2009).
[40] P. Nalbach and V. Leyton, Phy. Rev. A, **98**, 023855 (2018).
[41] J. T. Seeley; M. J. Richard; P. J. Love, J. Chem. Phys., **137**, 224109 (2012).
[42] S. B. Bravyi, A. Y. Kitaev, Ann. Physics, **298**, 210-226 (2002).
[43] P. J. J. O'Malley, R. Babbush, I. D. Kivlichan, J. Romero, J. R. McClean, R. Barends, J. Kelly, P. Roushan, A. Tranter, N. Ding et al., Phys. Rev. X, **6**, 031007 (2016).
[44] S. Majumder, C.G. Yale, T. D. Morris, D.S. Lobster, A.D. Burch, M.H.H Chow, M. C. Revelle, S. M. Clark, and R. C. Pooser, Quantum, **7**, 1006 (2023).
[45] F. Dominguez, J. Unger, M. Traube, B. Mant, C. Ertler, W. Lechner, Frontiers in Quantum Science and Technology, **2**, 1 (2023).
[46] S. Abel, Steve, J. C. Criado, and M. Spannowsky, Phys. Rev. A, **106**, 022601 (2022).
[47] Refer to the derivation of Eq. (S23) from section IV in Supplementary Material. The comparison with numerical results is discussed in detail in the subsection of optimal kick angle from Sec. VII in supplementary numerical results.
[48] See Figure S1 from Sec. VIII in Supplementary Material.
[49] See discussion from Eqs.(S18),(S19), and S(20) in Sec. IV of Supplementary Material.
[50] See Figure S3 from Sec. VIII in Supplementary Material.
[51] See Table I in Sec. I: Hydrogen Molecule Data in Supplementary Material.
[52] See Figure S2 from Sec. VIII in Supplementary Material.
[53] See Figure S4 and Figure S5 from Sec. VIII in Supplementary Material.
[54] Q. Sun, T. C. Berkelbach, N. S. Blunt, G. H. Booth, S. Guo, Z. Li, J. Liu, J. D. McClain, E. R. Sayfutyarova, S. Sharma et al., Wiley Interdiscip. Rev. Comput. Mol. Sci., **8**, e1340 (2018).
[55] M. Schuld and F. Petruccione, "Information encoding," in Supervised Learning With Quantum Computers. Cham, Switzerland: Springer, 2018, pp. 139–171.